

This discussion paper is/has been under review for the journal Atmospheric Chemistry and Physics (ACP). Please refer to the corresponding final paper in ACP if available.

## TransCom N<sub>2</sub>O model inter-comparison, Part II: Atmospheric inversion estimates of N<sub>2</sub>O emissions

R. L. Thompson<sup>1,2</sup>, K. Ishijima<sup>3</sup>, E. Saikawa<sup>4,5</sup>, M. Corazza<sup>6</sup>, U. Karstens<sup>7</sup>,  
P. K. Patra<sup>3</sup>, P. Bergamaschi<sup>6</sup>, F. Chevallier<sup>2</sup>, E. Dlugokencky<sup>8</sup>, R. G. Prinn<sup>4</sup>,  
R. F. Weiss<sup>9</sup>, S. O'Doherty<sup>10</sup>, P. J. Fraser<sup>11</sup>, L. P. Steele<sup>11</sup>, P. B. Krummel<sup>11</sup>,  
A. Vermeulen<sup>12</sup>, Y. Tohjima<sup>13</sup>, A. Jordan<sup>7</sup>, L. Haszpra<sup>14,15</sup>, M. Steinbacher<sup>16</sup>,  
S. Van der Laan<sup>17</sup>, T. Aalto<sup>18</sup>, F. Meinhardt<sup>19</sup>, M. E. Popa<sup>7,20</sup>, J. Moncrieff<sup>21</sup>, and  
P. Bousquet<sup>2</sup>

<sup>1</sup>Norwegian Institute for Air Research, Kjeller, Norway

<sup>2</sup>Laboratoire des Sciences du Climat et l'Environnement, Gif sur Yvette, France

<sup>3</sup>Research Institute for Global Change, JAMSTEC, Yokohama, Japan

<sup>4</sup>Center for Global Change Science, MIT, Cambridge, MA, USA

<sup>5</sup>Emory University, Atlanta, GA, USA

<sup>6</sup>Institute for Environment and Sustainability, JRC, Ispra, Italy

<sup>7</sup>Max Planck Institute for Biogeochemistry, Jena, Germany

<sup>8</sup>NOAA Earth System Research Laboratory, Global Monitoring Division, Boulder, CO, USA

<sup>9</sup>Scripps Institution of Oceanography, La Jolla, CA, USA

5271

<sup>10</sup>Atmospheric Chemistry Research Group, School of Chemistry, University of Bristol, Bristol, UK

<sup>11</sup>Centre for Australian Weather and Climate Research, CSIRO, Marine and Atmospheric Research, Aspendale, Victoria, Australia

<sup>12</sup>Energy Research Centre of the Netherlands (ECN), Petten, the Netherlands

<sup>13</sup>National Institute for Environmental Studies, Tsukuba, Japan

<sup>14</sup>Hungarian Meteorological Service, Budapest, Hungary

<sup>15</sup>Geodetic and Geophysical Institute, Research Centre for Astronomy and Earth Sciences, Hungarian Academy of Sciences, Sopron, Hungary

<sup>16</sup>Swiss Federal Laboratories for Materials Science and Technology (Empa), Duebendorf, Switzerland

<sup>17</sup>University of Groningen, Groningen, the Netherlands

<sup>18</sup>Finnish Meteorological Institute, Helsinki, Finland

<sup>19</sup>Umweltbundesamt, Messstelle Schauinsland, Kirchzarten, Germany

<sup>20</sup>University of Utrecht, Utrecht, the Netherlands

<sup>21</sup>University of Edinburgh, Edinburgh, UK

Received: 15 November 2013 – Accepted: 5 February 2014 – Published: 27 February 2014

Correspondence to: R. L. Thompson (rona.thompson@nilu.no)

Published by Copernicus Publications on behalf of the European Geosciences Union.



atmospheric inversion approach is that it provides a constraint on the total N<sub>2</sub>O emission since the atmosphere integrates the fluxes and requires that the change in atmospheric N<sub>2</sub>O abundance be balanced by the sum of its sources and sinks. In general terms, up-scaling approaches provide a detailed picture of the processes and source types while top-down approaches provide an integrated picture of the regional and long-term emissions and a check on the total budget. However, atmospheric inversions also have sources of error. The estimated fluxes are sensitive to errors in the modelled transport and, to varying degrees, the chemistry, as these are non-random errors that are extremely difficult to estimate and account-for in an inversion framework. Particularly for N<sub>2</sub>O, errors in stratosphere–troposphere exchange (STE) represent an important source of model error since there is a strong N<sub>2</sub>O mole fraction gradient across the tropopause owing to the loss of N<sub>2</sub>O through photolysis and reaction with O(<sup>1</sup>D) in the stratosphere (see Part I, Thompson et al., 2014b).

Part I of the TransCom N<sub>2</sub>O experiment examined the importance of atmospheric transport and surface fluxes on tropospheric N<sub>2</sub>O mole fractions and, specifically, looked at the influence of transport model errors on N<sub>2</sub>O mole fractions on seasonal to annual timescales (Thompson et al., 2014b). In this paper (Part II), we present N<sub>2</sub>O emission estimates from 5 inversion frameworks based on 5 different atmospheric chemistry transport models (CTMs), all of which also participated in Part I. In this context, the objectives of this paper are to:

- compare the posterior emissions from all inversions in a standardized way;
- analyse the emissions in terms of spatial distribution, seasonal variability, and to identify robust features common to all inversions;
- identify regions where there are discrepancies between inversions and their cause;
- present regional emissions estimates and their uncertainties.

5275

This paper is divided into four main sections. In Sect. 2, we outline the inversion frameworks and CTMs, as well as the prior flux estimates and atmospheric observations used in this study. Section 3.1 presents a validation of the inversion results by comparing the mole fractions simulated using the posterior fluxes with observations while Sect. 3.2 analyses the spatial and temporal distribution of the posterior fluxes. In Sect. 3.3, we compare these estimates with those of previous studies and conclude with a discussion of the major challenges for estimating N<sub>2</sub>O emissions from atmospheric inversions.

## 2 Methods

### 2.1 Inversion frameworks

Five different inversion frameworks participated in Part II of this experiment. In this paper, we refer to each of the frameworks according to the CTM used followed by “-I” to indicate that this is the inversion framework. Although the frameworks may be used with a different CTM, in this study the naming is unambiguous as a different CTM was used with each one (see Table 1). All frameworks use the Bayesian inversion method to find the optimal surface fluxes, that is, the fluxes that provide the best fit to the atmospheric observations,  $\mathbf{y}$ , while being guided by the prior flux estimates,  $\mathbf{x}_b$ , and their uncertainties (for details about the Bayesian method refer to Tarantola, 2005). Based on Bayesian theory, and Gaussian-error hypotheses, the optimal fluxes are those that minimize the cost function:

$$J(\mathbf{x}) = (\mathbf{x} - \mathbf{x}_b)^T \mathbf{B}^{-1} (\mathbf{x} - \mathbf{x}_b) + (H(\mathbf{x}) - \mathbf{y})^T \mathbf{R}^{-1} (H(\mathbf{x}) - \mathbf{y}) \quad (1)$$

where the prior flux uncertainties are described by the error covariance matrix,  $\mathbf{B}$ , the observation uncertainties are described by the error covariance matrix,  $\mathbf{R}$ , and  $H$  is an operator of the atmospheric transport and chemistry as defined by the CTM in each inversion framework. Depending on the inversion framework,  $H$  is either a matrix or

5276



biogeochemistry model (Dutreuil et al., 2009), which provides inter-annually varying fluxes at monthly and  $1.0^\circ \times 1.0^\circ$  resolution. For waste, fuel combustion, and industrial emissions, we used EDGAR-4.1 (Emission Database for Greenhouse gas and Atmospheric Research, available at: <http://edgar.jrc.ec.europa.eu/index.php>), which are  
5 estimated for the reference year 2005 and were provided annually at  $1.0^\circ \times 1.0^\circ$  resolution. Biomass burning estimates from GFED-2.1 (Global Fire Emissions Database) (van der Werf et al., 2010) were used, which were provided monthly and at  $1.0^\circ \times 1.0^\circ$  resolution. In total, the global emission for 2005 to 2009 was 16.8, 16.3, 16.8, 16.2 and 16.4 TgNyr<sup>-1</sup>, respectively.

### 10 2.2.3 Degrees of freedom

The number of degrees of freedom in the inversion is an important factor for determining how closely the posterior fluxes resemble the prior ones. For MOZART4-I and ACTMt42I67-I, which solve the inversion using coarse regions, the number of degrees of freedom is substantially reduced representing a strong constraint on the inversion  
15 as only the mean flux in each region is optimized and the flux pattern within each region remains as described a priori. On the other hand, solving for fine regions i.e. at the resolution of the transport model, as in TM5-I, TM3-I and LMDZ4-I, benefits from additional regularization constraints, such as spatial correlations of the prior flux errors (used in the definition of **B**). For TM5-I the spatial correlation length (200 km)  
20 means that the grid cells are only weakly correlated to one another resulting in a weak constraint, whereas in LMDZ4-I, longer scale lengths are used (500 km for land and 1000 km for ocean) resulting in a stronger constraint (see Table 2).

## 2.3 Atmospheric observations

Atmospheric observations of N<sub>2</sub>O mole fractions (nmolmol<sup>-1</sup> equivalently parts-per-billion, abbreviated as ppb) were pooled from two global networks, NOAA CCGG  
25 (Carbon Cycle and Greenhouse Gases) and AGAGE (Advanced Global Atmospheric

5279

Gases Experiment), as well as from a number of smaller regional networks and independent stations (see Fig. 1 and Table 4). From the NOAA CCGG network, 42 sites were included. Approximately weekly discrete air samples are taken at these sites, which are subsequently analysed for N<sub>2</sub>O using GC-ECD (Gas Chromatography Electron Capture Detector). These data are reported on the NOAA-2006A calibration scale  
5 (Hall et al., 2007) and have a reproducibility of 0.4 ppb based on the mean difference of flask pairs. The AGAGE network consists of 5 in-situ GC-ECD instruments. These data are reported on the SIO-1998 scale and have a reproducibility of approximately 0.1 ppb (Prinn et al., 2000). The MPI-BGC (Max Planck Institute for Biogeochemistry) network  
10 consists of 3 sites for discrete air samples and 2 sites with in-situ GC-ECD instruments. These data are also reported on the NOAA-2006A scale and have a reproducibility of about 0.3 ppb. In addition, data from 9 independently run stations with in-situ GC-ECD instruments were included (see Table 4).

These stations do not all use the same calibration scale and, thus, offsets exist between the measurements. Furthermore, even in the case where the measurements are reported on the same scale, there still may be offsets owing to systematic errors. These offsets can introduce significant errors in the optimized fluxes if they are not accounted for prior to, or in, the inversion. For this reason, calibration offsets were estimated using inter-calibration data for each of the in-situ stations, and for the 3 MPI-BGC flask sites  
15 together, relative to the NOAA-2006A scale (see Table 5). Since the inter-calibration data were not complete for all times and all sites, the offsets were included into the optimization problem in inversion frameworks with this capacity (i.e. in LMDZ4-I and TM5-I, and only TM5-I resolves the offsets temporally using annual resolution). In this case, the best estimates of the offsets were used as prior values. In the case that they  
20 could not be optimized (i.e. in MOZART4-I, ACMTt42I67-I, and TM3-I) the given values were used to correct the observations prior to the inversion.

5280









region are only constrained by the 2 in-situ sites, HAT and COI, and by the discrete sampling sites, BKT, GMI, LLN, and TAP. Second, since the prior flux uncertainties are calculated proportionally to the prior flux, the prior uncertainty for this region is large allowing the inversions considerable freedom to adjust the fluxes here. Lastly, differences in the modelled transport, such as the tropical convection, monsoon flow, and shifts in the North Pacific storm track, which are important in determining outflow from the Asian continent (Stohl et al., 2002) may also contribute to the disparity among emission estimates for South Asia. Stohl et al. (2002) showed that tracers emitted in Asia south of 30° N, particularly in India, are readily transported toward the ITCZ and thus could be one reason why LMDZ4-I, with a fast inter-hemispheric mixing rate, predicts the highest emissions for South Asia. Similar reasoning also applies to the large discrepancy for South and Tropical America. South and Tropical America is very poorly covered by the observation network (see Fig. 1) and the prior flux uncertainty for this region is very large. The posterior emission estimates for this region are also likely to be sensitive to features of the modelled transport, in particular, convective transport.

Unlike for the land regions, there is reasonably good agreement among inversions for the ocean regions. All ocean regions satisfy the second criterion, and only the region 30° S–30° N does not also satisfy the first criterion. The emissions for the Southern Ocean (90–30° S) were found to be smaller than estimated a priori, contributing 6% (median posterior value) to the global total, while emissions for the tropical (30° S–30° N) and northern (30–90° N) ocean regions, the emissions were found to be larger, contributing 22% and 7% to the global total, respectively.

### 3.2.3 Seasonal variability

The mean seasonal cycle for each of the 7 land and 3 ocean regions was calculated by averaging the total monthly emissions over the period 2006 to 2008 and is shown in Fig. 10. For the Northern Hemisphere temperate land regions, Europe, North America and North Asia, the prior flux seasonal cycle predicts a late summer maximum, i.e. between July and August. However, all inversions estimate smaller emissions in July

5287

and/or August relative to the prior. ACTMt42167-I and LMDZ4-I both estimate an earlier and broader maximum, between April and June, while MOZART4-I, TM5-I and TM3-I predict a broader maximum between June and July. In Part I of the inter-comparison, it was shown in the CTM integrations using fluxes with a late summer maximum worsened the fit to the atmospheric observations compared to using fluxes with no seasonal cycle. The result for the Northern Hemisphere temperate regions in this study confirms the hypothesis in Part I, that elevated emissions begin in earlier in spring and continue until autumn without a peak in late summer. This is in line with what is expected based on the dependence of N<sub>2</sub>O fluxes on soil moisture (measured by water-filled-pore-space, WFPS), soil temperature and the availability of nitrogen substrates, particularly NO<sub>3</sub><sup>-</sup> and NH<sub>4</sub><sup>+</sup> in soils (Butterbach-Bahl et al., 2013, and references therein). N<sub>2</sub>O flux is maximised with WFPS of between approximately 70–90% and has positive correlation with soil temperature (Smith et al., 1998). Therefore, low soil N<sub>2</sub>O flux is expected throughout winter and higher N<sub>2</sub>O is expected in summer so long as there is sufficient soil moisture and nitrogen substrate. N-fertilization usually occurs in spring and mid-summer providing sufficient nitrogen substrate but drier soils in late summer may limit N<sub>2</sub>O fluxes.

For the region of South Asia, there is some indication in the posterior fluxes of a double maximum, i.e. in ACTMt42167-I, TM5-I, and LMDZ4-I occurring in April and September. This approximately corresponds to the start and end of the Asian monsoon season, which lasts from April to September, while the period of lowest fluxes, from October to March, corresponds to the cool-dry season. This is in accordance with what has been found from in-situ flux measurements in sub-tropical Southern China, which experiences annual monsoons, that is, that WFPS, soil NO<sub>3</sub><sup>-</sup> and NH<sub>4</sub><sup>+</sup> content, and N<sub>2</sub>O fluxes were significantly higher in the hot-humid season than in the cool-dry season (Lin et al., 2010). However, the peak in spring may also partially be an artefact needed to compensate for the too low simulated spring atmospheric mole fraction as compared to the observations owing to a too strong influence of STT.

For the Southern Hemisphere regions of South and Tropical America and Africa, there is very little seasonality in the prior fluxes. However, all of the inversions estimate a March–April minimum for South and Tropical America and similarly (except LMDZ4-I) for Africa. For South and Tropical America, the March–April minimum is not easy to explain in terms of soil N<sub>2</sub>O fluxes. In fact, from the few existing regional measurements of N<sub>2</sub>O fluxes in tropical South America only a small seasonal cycle has been observed with elevated fluxes during the wet season from March–May (D’Amelio et al., 2009). Therefore, it is likely that the minimum in the optimized fluxes is due to transport errors since the timing of the atmospheric N<sub>2</sub>O minimum in April, determined to a large extent by STT, is not captured by the models, thus to match observations, the inversions estimate lower N<sub>2</sub>O emissions at this time. It is possible that the impact of this transport error on the optimized fluxes would not be so strong if there were better observational constraints for South America. The same also applies for Africa where the minimum in March–April cannot be explained in terms of variability in soil fluxes as this time corresponds to the wet season when the highest N<sub>2</sub>O emissions are expected.

For the ocean regions, the phase and amplitude of the seasonal cycles a posteriori differ little from that a priori. In the Southern Ocean, the minimum in April and maximum in September–October is consistent with the independent estimate of Nevison et al. (2005) and is largely driven by the upwelling and subsequent venting of subsurface water, which is enriched in N<sub>2</sub>O. In the tropical and northern ocean regions, the seasonal cycle is much smaller in amplitude but is also likely driven by seasonal changes in upwelling.

### 3.3 Comparison with other estimates

To put this study into context with previous work, we compare our results to independent N<sub>2</sub>O emission estimates. We have chosen 5 studies, including 2 atmospheric inversions (Hirsch et al., 2006; Huang et al., 2008) and 3 inventory and model-based estimates (Denman et al., 2007; Syakila and Kroeze, 2011; Zaehle et al., 2011), which are global in coverage and include estimates of N<sub>2</sub>O emissions from all sources and

5289

are thus appropriate for this comparison. (The study of Zaehle et al. (2011) is not completely independent as it uses the same terrestrial biosphere model, O-CN, for the estimate of N<sub>2</sub>O soil emissions as was used in this study’s prior emissions, however, the O-CN simulations used different climate forcing and N-deposition.) Figure 11 compares the global, land, and ocean total emissions, as well as the emission distribution by semi-hemisphere, where available. Although the exact period of each study varies, they all include estimates of the global N<sub>2</sub>O budget in the 2000s. At the global scale, all estimates agree within the range of uncertainties (no uncertainty estimate was provided by Syakila and Kroeze (2011)). Progress, however, has been made in reducing the level of uncertainty from 4.5 TgNyr<sup>-1</sup> in the IPCC AR4 (Intergovernmental Panel on Climate Change Fourth Assessment Report, 2007) to 0.7 TgNyr<sup>-1</sup> in this study (1σ, 68 % probability assuming Gaussian error distribution) with the complete range of inversions from 16.1 to 18.7 TgNyr<sup>-1</sup>. Previous studies differ in the apportionment between land and ocean emissions, with ocean estimates varying from 24 % to 38 % of the global total, whereas we found fairly good agreement among the inversions participating in this study with ocean estimates varying between 31 % and 38 % of the global total. At the semi-hemisphere scale, we find a few important differences between our median estimates and previous ones: for the region 90° S to 30° S we estimate higher emissions (7 % of the global total), for the region 0° to 30° N we estimate lower emissions (41 %), and for 30° N to 90° N slightly higher emissions (23 %). Comparing the ratio for emissions in the regions 0° to 30° N and 30° N to 90° N, all our inversions give a lower value (from 1.5 to 1.9) compared with 3.0 (Hirsch et al., 2006) and 2.9 (Huang et al., 2008) for the periods 1998–2005 and 2001–2005, respectively. Since our estimates are for a later period (2006–2008), this difference may reflect real changes in emissions. It is known that emissions have been increasing in Asia, particularly, in China, over the past decade, which has also increased the overall emission in the region 30° N to 90° N, while no significant trends have been found in other regions (Thompson et al., 2014a). The increase in China has primarily been driven by

an increase in N-fertilizer usage and to a lesser extent, an increase in industrial and combustion sources of N<sub>2</sub>O (Thompson et al., 2014a).

#### 4 Summary and conclusions

In this study we have compared the N<sub>2</sub>O emission estimates of 5 inversion frameworks and analysed these in terms of their spatial distribution and seasonal variability. In general, there is a high level of agreement among the 5 inversions participating in this study despite the differences in inversion approach, atmospheric transport model and meteorological data used. This gives us confidence that there has been substantial progress made in terms of uncertainty reduction. Moreover, we have identified emission patterns that are robust, that is, common to all inversion frameworks as well as those that depend strongly on the modelled transport and/or inversion set-up. The salient results are summarized as follows:

- the mean global annual N<sub>2</sub>O emission ranges between 16.1 and 18.7 with a median and MAD of 16.7 and 0.7 Tg Nyr<sup>-1</sup>, respectively for the years 2006 to 2008;
- ocean emissions were found to contribute between 31 % and 38 % and land emissions between 62 % and 69 % to the global total;
- the apportionment of emissions to each semi-hemisphere was fairly close among inversions, with 7 ± 1 % to 90–30° S, 28 ± 2 % to 30–0°, 41 ± 1 % to 0–30° N and 23 ± 1 % to 30–90° N (median and MAD as a percentage of the global total), thus making the Northern Hemisphere tropics and subtropics the most important latitudinal range for N<sub>2</sub>O emissions globally;
- all inversions estimated lower emissions for the latitudes 90–30° S relative to the prior, however, the median estimate (7 % of the global total) was still higher than that found in previous studies (0 to 4 %);

5291

- the ratio of emissions in 0–30° N to 30–90° N is smaller in all inversions (range of 1.52 to 1.91 and median of 1.9) compared to previous studies (2.9 and 3.0), representing a change in the percentage of the global total of –16 % for 0–30° N and of +3 % for 30–90° N;
- all inversions estimated higher emissions in Europe and Africa relative to the prior, contributing 6 % (1.04 ± 0.20 Tg Nyr<sup>-1</sup>) and 20 % (3.36 ± 0.04 Tg Nyr<sup>-1</sup>) (median and MAD values), respectively to the global total compared with 5 % (0.80 Tg Nyr<sup>-1</sup>) and 18 % (3.07 Tg Nyr<sup>-1</sup>) a priori;
- all inversions (except LMDZ4) estimate lower emissions in North America contributing 4 % (0.74 ± 0.11 Tg Nyr<sup>-1</sup>) (median values) to the global total compared to 6 % (1.00 Tg Nyr<sup>-1</sup>) a priori;
- all inversions (except TM5) estimate lower emissions in South and Tropical America contributing 14 % (2.33 ± 0.27 Tg Nyr<sup>-1</sup>) to the global total compared to 15 % (2.55 Tg Nyr<sup>-1</sup>) a priori;
- the largest uncertainties were found in the estimates for South and Tropical America and South Asia owing to uncertainties in the modelled atmospheric transport and to the poor observational constraint for these regions.

In general, the global N<sub>2</sub>O budget, the total emissions and their spatial distribution, are close to what has been found from previous studies. One notable difference in our inversion estimates compared to previous ones though, is the shift in the distribution in the Northern Hemisphere, with lower emissions in the tropics and subtropics and higher emissions in temperate latitudes. Moreover, our inversions show a convergence of estimates both at the global and sub-continental scale. This good agreement is most likely due to the expansion of the atmospheric observation network. However, considerable uncertainties remain, especially in the less well-constrained regions of South Asia and South and Tropical America. These regions also appear to be very sensitive to uncertainties in the modelled atmospheric transport. Also sensitive to atmospheric transport,

5292



- Geels, C., Gloor, M., Ciais, P., Bousquet, P., Peylin, P., Vermeulen, A. T., Dargaville, R., Aalto, T., Brandt, J., Christensen, J. H., Frohn, L. M., Haszpra, L., Karstens, U., Rödenbeck, C., Ramonet, M., Carboni, G., and Santaguida, R.: Comparing atmospheric transport models for future regional inversions over Europe – Part 1: mapping the atmospheric CO<sub>2</sub> signals, *Atmos. Chem. Phys.*, 7, 3461–3479, doi:10.5194/acp-7-3461-2007, 2007.
- 5 Gloor, M., Dlugokencky, E., Brenninkmeijer, C., Horowitz, L., Hurst, D. F., Dutton, G., Crevoisier, C., Machida, T., and Tans, P.: Three-dimensional SF<sub>6</sub> data and tropospheric transport simulations: signals, modeling accuracy, and implications for inverse modeling, *J. Geophys. Res.*, 112, D15112, doi:10.1029/2006jd007973, 2007.
- 10 Hall, B. D., Dutton, G. S., and Elkins, J. W.: The NOAA nitrous oxide standard scale for atmospheric observations, *J. Geophys. Res.*, 112, D09305, doi:10.1029/2006jd007954, 2007.
- Hirsch, A. I., Michalak, A. M., Bruhwiler, L. M., Peters, W., Dlugokencky, E. J., and Tans, P. P.: Inverse modeling estimates of the global nitrous oxide surface flux from 1998–2001, *Global Biogeochem. Cy.*, 20, GB1008, doi:10.1029/2004gb002443, 2006.
- 15 Huang, J., Golombek, A., Prinn, R., Weiss, R., Fraser, P., Simmonds, P., Dlugokencky, E. J., Hall, B., Elkins, J., Steele, P., Langenfelds, R., Krummel, P., Dutton, P., and Porter, L.: Estimation of regional emissions of nitrous oxide from 1997 to 2005 using multinet network measurements, a chemical transport model, and an inverse method, *J. Geophys. Res.*, 113, D17313, doi:10.1029/2007JD009381, 2008.
- 20 Kort, E. A., Patra, P. K., Ishijima, K., Daube, B. C., Jimenez, R., Elkins, J., Hurst, D., Moore, F. L., Sweeney, C., and Wofsy, S. C.: Tropospheric distribution and variability of N<sub>2</sub>O: evidence for strong tropical emissions, *Geophys. Res. Lett.*, 38, L15806, doi:10.1029/2011gl047612, 2011.
- Lin, S., Iqbal, J., Hu, R., and Feng, M.: N<sub>2</sub>O emissions from different land uses in mid-subtropical China, *Agr. Ecosyst. Environ.*, 136, 40–48, doi:10.1016/j.agee.2009.11.005, 2010.
- Minschwaner, K., Salawitch, R. J., and McElroy, M. B.: Absorption of solar radiation by O<sub>2</sub>: implications for O<sub>3</sub> and lifetimes of N<sub>2</sub>O, CFC<sub>3</sub>, and CF<sub>2</sub>Cl<sub>2</sub>, *J. Geophys. Res.*, 98, 10543–10561, 1993.
- 30 Nevison, C. D., Keeling, R. F., Weiss, R. F., Popp, B. N., Jin, X., Fraser, P. J., Porter, L. W., and Hess, P. G.: Southern Ocean ventilation inferred from seasonal cycles of atmospheric N<sub>2</sub>O and O<sub>2</sub>/N<sub>2</sub> at Cape Grim, Tasmania, *Tellus B*, 57, 218–229, 2005.

5295

- Olivier, J. G. J., Van Aardenne, J. A., Dentener, F., Pagliari, V., Ganzeveld, L. N., and Peters, J. A. H. W.: Recent trends in global greenhouse gas emissions: regional trends 1970–2000 and spatial distribution of key sources in 2000, *Environ. Sci.*, 2, 81–99, doi:10.1080/15693430500400345, 2005.
- 5 Park, S., Croteau, P., Boering, K. A., Etheridge, D. M., Ferretti, D., Fraser, P. J., Kim, K. R., Krummel, P. B., Langenfelds, R. L., van Ommen, T. D., Steele, L. P., and Trudinger, C. M.: Trends and seasonal cycles in the isotopic composition of nitrous oxide since 1940, *Nat. Geosci.*, 5, 261–265, 2012.
- 10 Patra, P. K., Houweling, S., Krol, M., Bousquet, P., Belikov, D., Bergmann, D., Bian, H., Cameron-Smith, P., Chipperfield, M. P., Corbin, K., Fortems-Cheiney, A., Fraser, A., Gloor, E., Hess, P., Ito, A., Kawa, S. R., Law, R. M., Loh, Z., Maksyutov, S., Meng, L., Palmer, P. I., Prinn, R. G., Rigby, M., Saito, R., and Wilson, C.: TransCom model simulations of CH<sub>4</sub> and related species: linking transport, surface flux and chemical loss with CH<sub>4</sub> variability in the troposphere and lower stratosphere, *Atmos. Chem. Phys.*, 11, 12813–12837, doi:10.5194/acp-11-12813-2011, 2011.
- 15 Prather, M. J., Holmes, C. D., and Hsu, J.: Reactive greenhouse gas scenarios: systematic exploration of uncertainties and the role of atmospheric chemistry, *Geophys. Res. Lett.*, 39, L09803, doi:10.1029/2012gl051440, 2012.
- 20 Prinn, R. G., Cunnold, D., Rasmussen, R., Simmonds, P., Alyea, F., Crawford, A., Fraser, P., and Rosen, R.: Atmospheric emissions and trends of nitrous oxide deduced from 10 years of ALE-GAGE data, *J. Geophys. Res.*, 95, 18369–18385, 1990.
- Prinn, R. G., Weiss, R. F., Fraser, P. J., Simmonds, P. G., Cunnold, D. M., Alyea, F. N., O'Doherty, S., Salameh, P., Miller, B. R., Huang, J., Wang, R. H. J., Hartley, D. E., Harth, C., Steele, L. P., Sturrock, G., Midgley, P. M., and McCulloch, A.: A history of chemically and radiatively important gases in air deduced from ALE/GAGE/AGAGE, *J. Geophys. Res.*, 105, 17751–17792, 2000.
- Ravishankara, A. R., Daniel, J. S., and Portmann, R. W.: Nitrous oxide (N<sub>2</sub>O): the dominant ozone-depleting substance emitted in the 21st century, *Science*, 326, 123–125, 2009.
- Rayner, P. J., Enting, I. G., Francey, R. J., and Langenfelds, R.: Reconstructing the recent carbon cycle from atmospheric CO<sub>2</sub>, δ<sup>13</sup>C and O<sub>2</sub>/N<sub>2</sub> observations, *Tellus B*, 51, 213–232, 1999.
- 30

5296

- Rödenbeck, C.: Estimating CO<sub>2</sub> sources and sinks from atmospheric mixing ratio measurements using a global inversion of atmospheric transport, Technical Report, Max Planck Institute for Biogeochemistry, Jena, Germany, 6, 2005.
- Saikawa, E., Prinn, R. G., Dlugokencky, E., Ishijima, K., Dutton, G. S., Hall, B. D., Langenfelds, R., Tohjima, Y., Machida, T., Manizza, M., Rigby, M., O'Doherty, S., Patra, P. K., Harth, C. M., Weiss, R. F., Krummel, P. B., van der Schoot, M., Fraser, P. B., Steele, L. P., Aoki, S., Nakazawa, T., and Elkins, J. W.: Global and regional emissions estimates for N<sub>2</sub>O, *Atmos. Chem. Phys. Discuss.*, 13, 19471–19525, doi:10.5194/acpd-13-19471-2013, 2013.
- Smith, K. A., Thomson, P. E., Clayton, H., McTaggart, I. P., and Conen, F.: Effects of temperature, water content and nitrogen fertilisation on emissions of nitrous oxide by soils, *Atmos. Environ.*, 32, 3301–3309, 1998.
- Stohl, A., Eckhardt, S., Forster, C., James, P., and Spichtinger, N.: On the pathways and timescales of intercontinental air pollution transport, *J. Geophys. Res.-Atmos.*, 107, 4684, doi:10.1029/2001jd001396, 2002.
- Syakila, A. and Kroeze, C.: The global nitrous oxide budget revisited, *Greenhouse Gas Measurement and Management*, 1, 17–26, 2011.
- Tarantola, A.: *Inverse Problem Theory and Methods for Model Parameter Estimation*, Society for Industrial and Applied Mathematics, Philadelphia, 2005.
- Thompson, R. L., Bousquet, P., Chevallier, F., Rayner, P. J., and Ciais, P.: Impact of the atmospheric sink and vertical mixing on nitrous oxide fluxes estimated using inversion methods, *J. Geophys. Res.*, 116, D17, doi:10.1029/2011jd015815, 2011a.
- Thompson, R. L., Gerbig, C., and Rödenbeck, C.: A Bayesian inversion estimate of N<sub>2</sub>O emissions for western and central Europe and the assessment of aggregation errors, *Atmos. Chem. Phys.*, 11, 3443–3458, doi:10.5194/acp-11-3443-2011, 2011b.
- Thompson, R. L., Chevallier, F., Crotwell, A. M., Dutton, G., Langenfelds, R. L., Prinn, R. G., Weiss, R. F., Tohjima, Y., Nakazawa, T., Krummel, P. B., Steele, L. P., Fraser, P., O'Doherty, S., Ishijima, K., and Aoki, S.: Nitrous oxide emissions 1999 to 2009 from a global atmospheric inversion, *Atmos. Chem. Phys.*, 14, 1801–1817, doi:10.5194/acp-14-1801-2014, 2014a.
- Thompson, R. L., Patra, P. K., Ishijima, K., Saikawa, E., Corazza, M., Karstens, U., Wilson, C., Bergamaschi, P., Dlugokencky, E., Sweeney, C., Prinn, R. G., Weiss, R. F., O'Doherty, S., Fraser, P. J., Steele, L. P., Krummel, P. B., Saunio, M., Chipperfield, M., and Bousquet, P.: TransCom N<sub>2</sub>O model inter-comparison – Part 1: Assessing the influence of transport and

5297

- surface fluxes on tropospheric N<sub>2</sub>O variability, *Atmos. Chem. Phys. Discuss.*, 14, 2307–2362, doi:10.5194/acpd-14-2307-2014, 2014b.
- van der Werf, G. R., Randerson, J. T., Giglio, L., Collatz, G. J., Mu, M., Kasibhatla, P. S., Morton, D. C., DeFries, R. S., Jin, Y., and van Leeuwen, T. T.: Global fire emissions and the contribution of deforestation, savanna, forest, agricultural, and peat fires (1997–2009), *Atmos. Chem. Phys.*, 10, 11707–11735, doi:10.5194/acp-10-11707-2010, 2010.
- Volk, C. M., Elkins, J. W., Fahey, D. W., Dutton, G. S., Gilligan, J. M., Loewenstein, M., Podolske, J. R., Chan, K. R., and Gunson, M. R.: Evaluation of source gas lifetimes from stratospheric observations, *J. Geophys. Res.*, 102, 25543–25564, 1997.
- Zaehle, S. and Friend, A. D.: Carbon and nitrogen cycle dynamics in the O-CN land surface model: 1. Model description, site-scale evaluation, and sensitivity to parameter estimates, *Global Biogeochem. Cy.*, 24, GB1005, doi:10.1029/2009gb003521, 2010.
- Zaehle, S., Ciais, P., Friend, A. D., and Prieur, V.: Carbon benefits of anthropogenic reactive nitrogen offset by nitrous oxide emissions, *Nat. Geosci.*, 4, 601–605, 2011.

5298



**Table 3.** Prior flux model overview (totals shown for 2005).

Category	Dataset	Resolution	Total (TgNyr <sup>-1</sup> )
terrestrial biosphere	ORCHIDEE O-CN	monthly	10.83
ocean	PISCES	monthly	4.28
waste water	EDGAR-4.1	annual	0.21
solid waste	EDGAR-4.1	annual	0.004
solvents	EDGAR-4.1	annual	0.05
fuel production	EDGAR-4.1	annual	0.003
ground transport	EDGAR-4.1	annual	0.18
industry combustion	EDGAR-4.1	annual	0.41
residential & other combustion	EDGAR-4.1	annual	0.18
shipping	EDGAR-4.1	annual	0.002
other sources	EDGAR-4.1	annual	0.0005
biomass burning	GFED-2	monthly	0.71
Total		monthly	16.84

5301

**Table 4.** Atmospheric observation sites using in the inversions. (F = Flask, C = Continuous). Altitude is specified as metres above sea-level (m a.s.l.).

ID	Station	Operator	Type	Latitude	Longitude	Altitude (m a.s.l.)
ALT	Alert, Canada	NOAA	F	82.5° N	62.5° W	210
ASC	Ascension Isl., UK	NOAA	F	7.9° S	14.4° W	54
ASK	Assekrem, Algeria	NOAA	F	23.2° N	5.4° E	2728
AZR	Azores, Portugal	NOAA	F	38.8° N	27.4° W	40
BAL	Baltic Sea, Poland	NOAA	F	55.4° N	17.2° E	7
BIK	Bialystok, Poland	MPI-BGC	C	55.3° N	22.8° E	460
BKT	Bukit Kototabang, Indonesia	NOAA	F	0.2° S	100.3° E	865
BME	St. Davis Head, Bermuda, UK	NOAA	F	32.4° N	64.7° W	30
BMW	Tudor Hill, Bermuda, UK	NOAA	F	32.3° N	64.9° W	30
BRW	Barrow, Alaska	NOAA	F	71.3° N	156.6° W	11
BSC	Black Sea, Romania	NOAA	F	44.2° N	28.7° E	3
CBA	Cold Bay, Alaska	NOAA	F	55.2° N	162.7° W	21
CBW	Cabauw, Netherlands	ECN	C	52.0° N	4.9° E	118
CGO	Cape Grim, Tasmania	AGAGE	C	40.7° S	144.7° E	164
CHR	Christmas Isl.	NOAA	F	1.7° N	157.2° W	3
COI	Cape Ochi-ishi, Japan	NIES	C	43.2° N	145.5° E	45
CRZ	Crozet Isl., France	NOAA	F	46.45° S	51.9° E	120
CVR	Calhau, Cape Verde	MPI-BGC	F	16.9° N	24.9° W	10
EIC	Easter Island, Chile	NOAA	F	27.2° S	109.5° W	50
GMI	Mariana Isl., Guam	NOAA	F	13.4° N	144.8° E	2
HAT	Hateruma, Japan	NIES	C	24.1° N	123.8° E	10
HBA	Halley Stn., Antarctica	NOAA	F	75.6° S	26.5° W	30
HUN	Hegyhatsal, Hungary	ELTE	C	46.9° N	16.7° E	344
ICE	Heimay, Iceland	NOAA	F	63.3° N	20.3° W	118
IZO	Tenerife, Spain	NOAA	F	28.3° N	16.5° W	2360
JFJ	Jungfrauoch, Switzerland	EMPA	C	46.6° N	8.0° E	3580
KEY	Key Biscayne, Florida	NOAA	F	25.7° N	80.2° W	3
KUM	Cape Kumukahi	NOAA	F	19.5° N	154.8° W	3
KZD	Sary Tauku, Kazakhstan	NOAA	F	44.1° N	76.8° E	601

5302







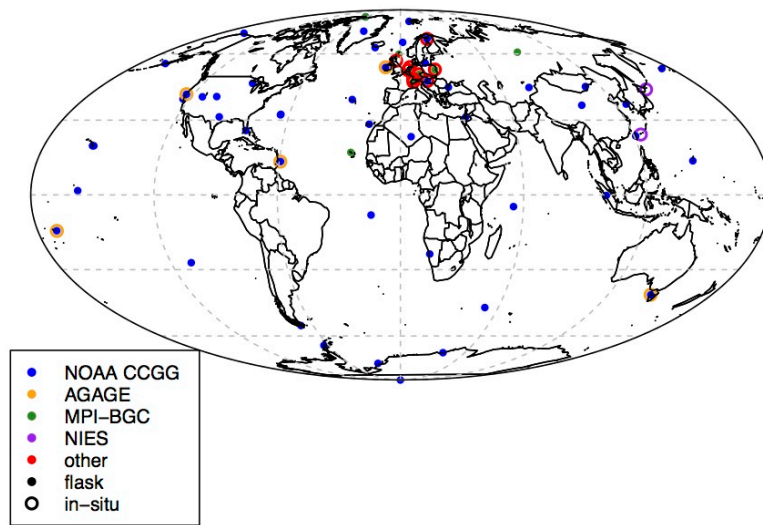


Fig. 1. Map of surface sites for atmospheric observations.

5307

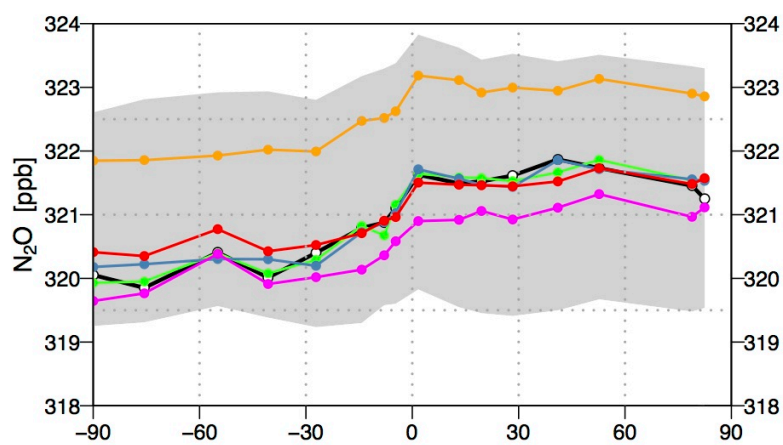
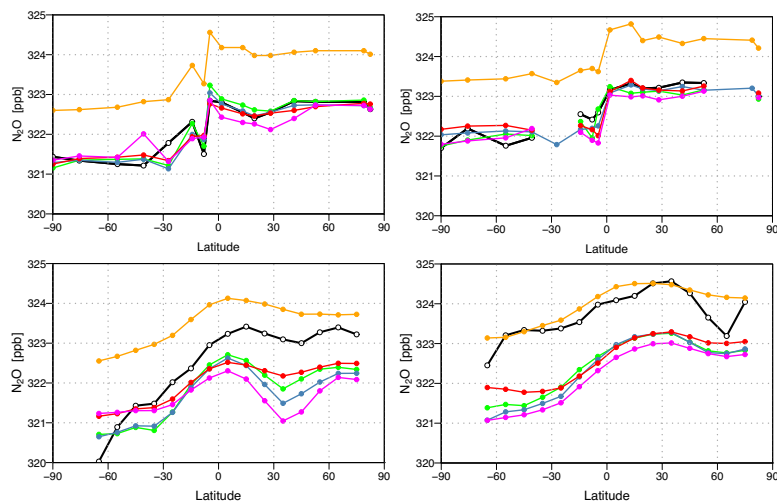


Fig. 2. Comparison of the annual mean  $N_2O$  gradient (ppb) for 2006 to 2009 with surface observations. The grey shaded area shows the range of values for the model using the prior fluxes. (Legend: observations, black; MOZART4, orange; ACTMt42l67, green; TM5, blue; TM3, red; LMDZ4, magenta.)

5308



**Fig. 3.** Comparison of model simulations with observations of  $\text{N}_2\text{O}$  mole fraction (ppb) from surface sites (upper) and pressure-weighted column averages (up to 10 000 m) from HIPPO aircraft profiles (lower) for January (left) and November (right) 2009. (Legend: observations, black; MOZART4, orange; ACTMt42l67, green; TM5, blue; TM3, red; LMDZ4, magenta.)

5309

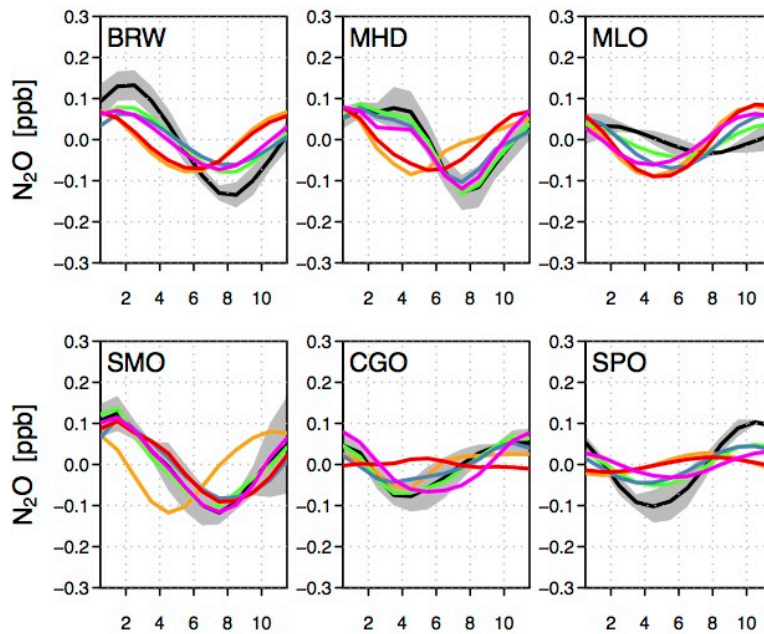


**Fig. 4.** Comparison of the mean (2006–2008) observed and simulated seasonal cycles in  $\text{N}_2\text{O}$  mole fraction (ppb) at selected key sites. The grey shaded indicates the range of uncertainty ( $1\sigma$  standard deviation) in the observations. For a description of the site abbreviations see Table 4. (Legend: observations, black; MOZART4, orange; ACTMt42l67, green; TM5, blue; TM3, red; LMDZ4, magenta.)

5310

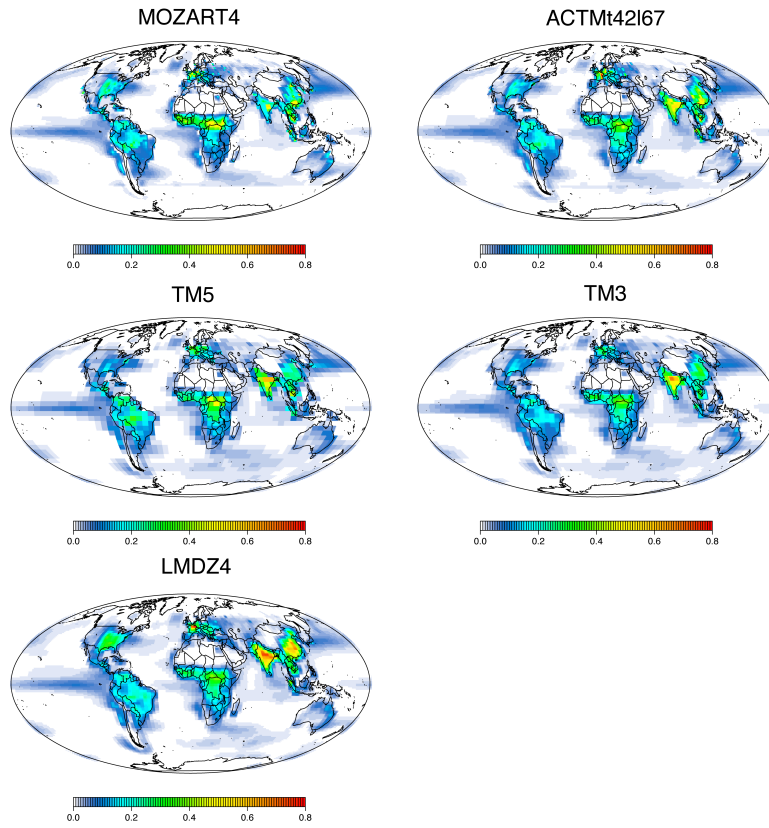


**Fig. 5.** Maps of annual mean posterior  $\text{N}_2\text{O}$  flux ( $\text{gNm}^{-2}\text{yr}^{-1}$ ) for 2006–2008.

5311

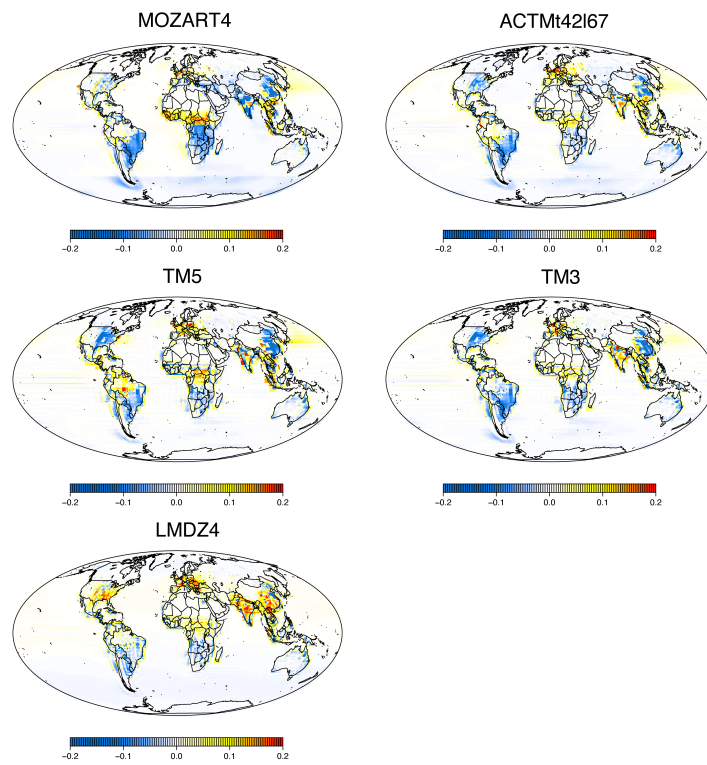


**Fig. 6.** Maps of annual mean flux increments for 2006–2008 ( $\text{gNm}^{-2}\text{yr}^{-1}$ ) relative to the prior fluxes.

5312



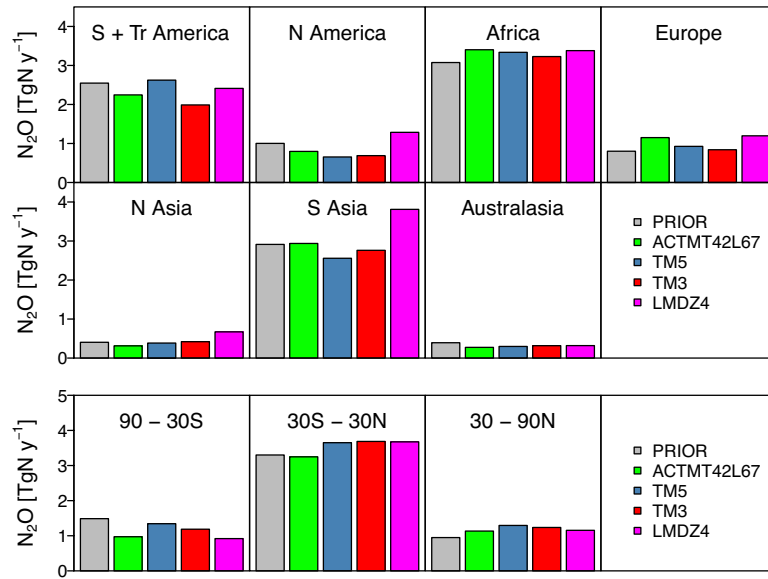


**Fig. 9.** Annual mean (2006–2008) regional emission estimates ( $\text{TgNyr}^{-1}$ ) for the 7 land and 3 ocean regions. The colours refer to the different inversion frameworks as indicated in the legend.

5315

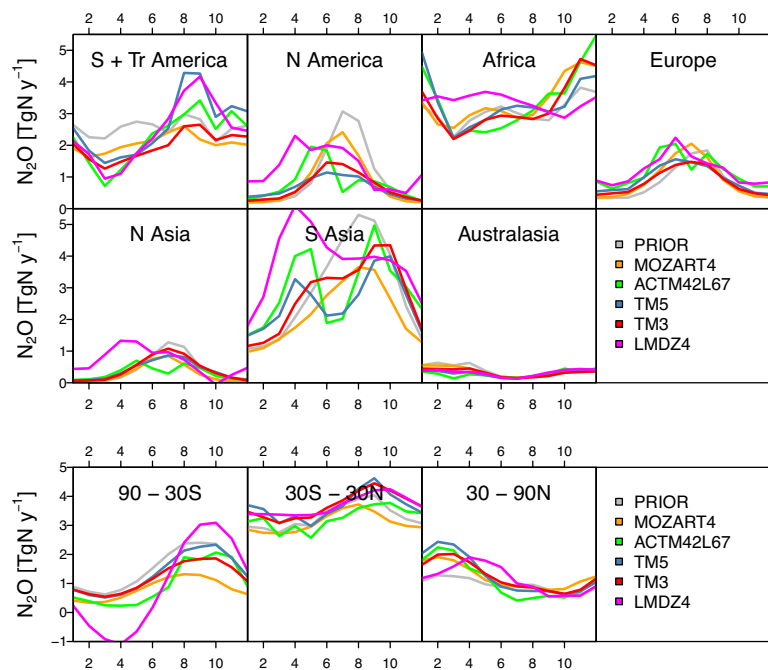


**Fig. 10.** Mean (2006–2008) seasonal cycle in  $\text{N}_2\text{O}$  flux ( $\text{TgNyr}^{-1}$ ) for each of the 7 sub-continental and 3 ocean regions.

5316

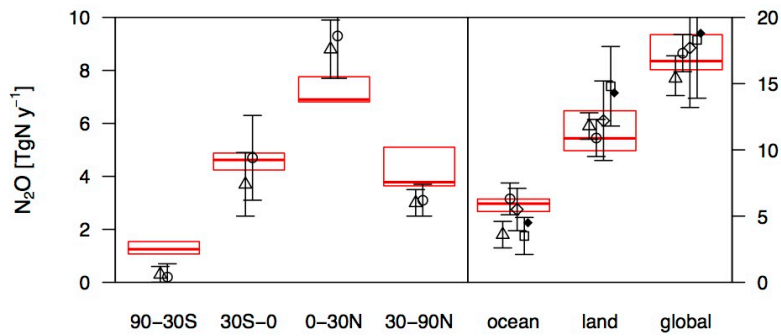


**Fig. 11.** Comparison of the total emissions for each semi-hemisphere region, the ocean, land and globally from this study with previous estimates. The vertical extents of the red boxes indicate the range and the horizontal lines in the interior indicate the median of inversion estimates from this study. The points indicate the values from previous studies: Hirsch et al. (2006), open circles; Huang et al. (2008), triangles; AR4, diamonds; Syakila et al. (2011), solid circles; Zaehle et al. (2011), squares. The error bars indicate the  $1\sigma$  uncertainty.

5317

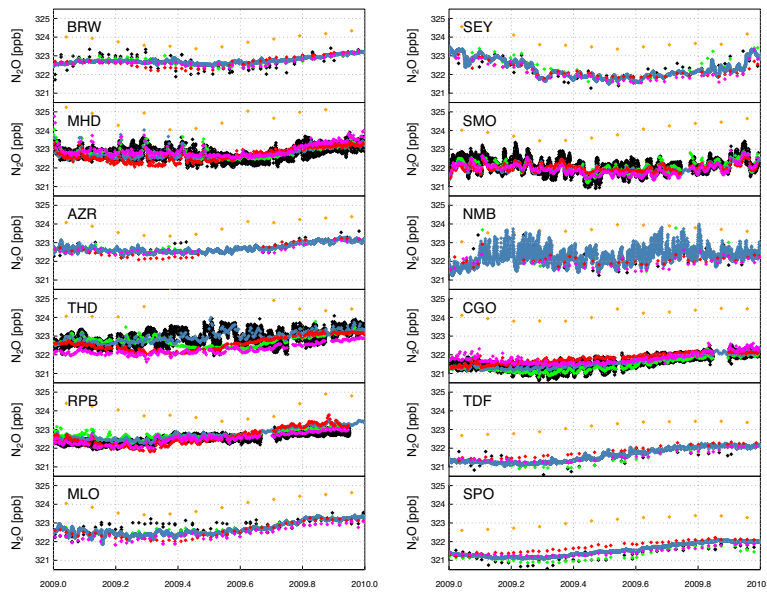


**Fig. A1.** Comparison of the daily mean  $N_2O$  mole fractions (ppb) simulated by integrating the CTMs with their corresponding posterior fluxes. Note for MOZART4 only monthly means were submitted. (Legend: observations, black; MOZART4, orange; ACTMt42l67, green; TM5, blue; TM3, red; LMDZ4, magenta.)

5318



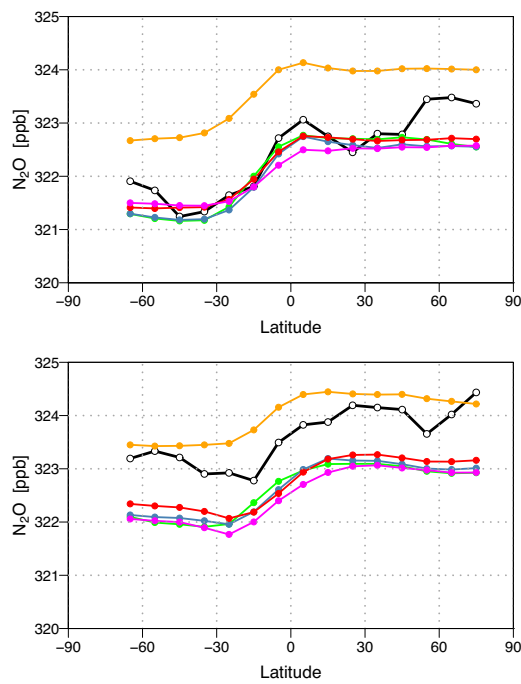


**Fig. A2.** Comparison of model simulations with pressure-weighted column averages from HIPPO aircraft profiles for January (top) and November (bottom) 2009. The column average was calculated from the surface up to 2000 m. (Legend: observations, black; MOZART4, orange; ACTMt42l67, green; TM5, blue; TM3, red; LMDZ4, magenta.)

5319

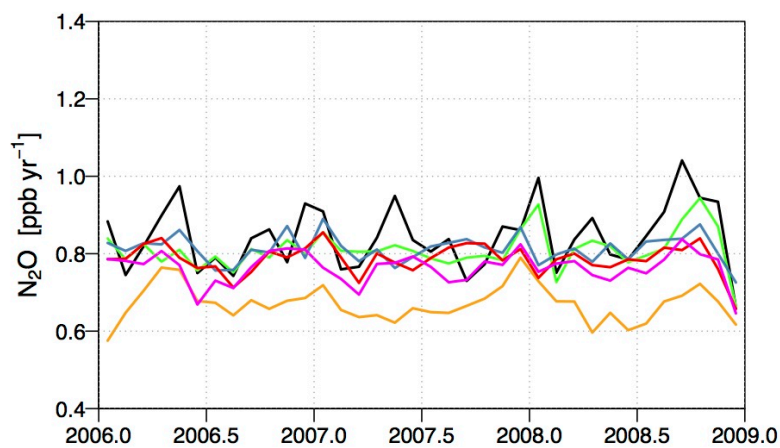


**Fig. A3.** Growth rate in atmospheric  $N_2O$  mole fraction ( $ppb\ yr^{-1}$ ). (Legend: observations, black; MOZART4, orange; ACTMt42l67, green; TM5, blue; TM3, red; LMDZ4, magenta.)

5320

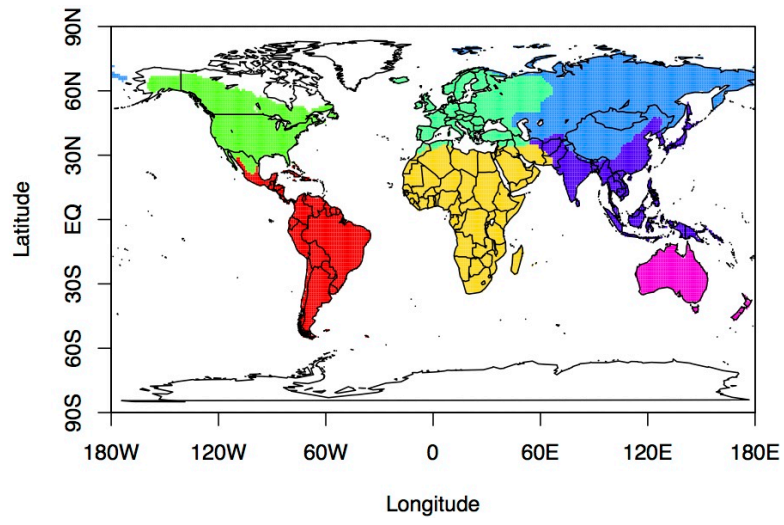


**Fig. A4.** Map of the 7 sub-continental regions used in the analysis. (North America = green, Tropical & South America = red, Africa = yellow, Europe = cyan, North Asia = blue, South Asia = purple, Australasia = magenta.)